Editors' Suggestion

Hidden magnetic phases in *i*-MAX compounds

Dror Yahav,[1] Ariel Maniv,[2] Daniel Potashnikov,[2] Asaf Pesach,[2] El'ad N. Caspi,[2] Arneil P. Reyes,[3] Quanzheng Tao,[4] Johanna Rosén,[4] and Eran Maniv[1]

[1]*Department of Physics, Ben-Gurion University of the Negev, Be'er-Sheva 84105, Israel*

[2]*Physics Department, NRCN, P.O. Box 9001, Be'er Sheva 84190, Israel*

[3]*National High Magnetic Field Laboratory, Tallahassee, Florida 32310, USA*

[4]*Materials Design, Department of Physics, Chemistry and Biology (IFM), Linköping University, SE-58183 Linköping, Sweden*

(Received 5 November 2024; revised 12 January 2025; accepted 24 January 2025; published 20 March 2025)

We uncover a high-field magnetic phase in *i*-MAX compounds exhibiting a canted antiferromagnetic order with unprecedented properties, revealed through NMR and AC susceptibility. Intriguingly, as the atomic number of rare earth increases, the transition field of this canted antiferromagnetic phase grows at the expense of the lower-field antiferromagnetic state. Our findings point to the complexity of the magnetic structure in *i*-MAX compounds, demonstrating a nontrivial evolution of their phase diagram while increasing both the atomic number of the rare-earth element and the external field.

DOI: 10.1103/PhysRevB.111.094427

I. INTRODUCTION

i-MAX compounds are in-plane ordered nanolaminated materials, based on the well known MAX phases [1]. In MAX phases M is an early transition metal, A is an A-group element, and X can be C, N, B, and/or P [2]. They have the general chemical formula $M_{n+1}AX_n$, where n is an integer number. These compounds have recently gained much interest, as they are parent compounds for 2D MXenes, which might be potentially interesting from several technological aspects, such as spintronics (magnetic MXenes) and energy storage, including improved batteries [3].

i-MAX compounds have the general chemical formula $(M_{2/3}M'_{1/3})_2AX$ where the M, and M′ elements are ordered within the M plane [4,5]. This ordering is accompanied by reduction in crystal symmetry from hexagonal in MAX phases to typically monoclinic, but still maintains the general MAX phase stacking of same element layers along the c axis. Most importantly, unlike in the case of MAX phase compounds, it was recently found that rare-earth (RE) elements can be introduced into the *i*-MAX M′ site [6]. This addition into the general MAX phase compounds opens a new set of magnetic properties that is characterized by high complexity of structures and strong dependency on the specific RE element, temperature, and magnetic field [6–10].

As noted in Barbier *et al.* [11], such compounds are expected to show a complicated magnetic structure, as a result of oscillating RKKY coupling of the 4f electrons of the different RE atoms through the conducting electron sea together with possible geometrical frustration due to the triangular RE lattice. Indeed, extensive measurements, done recently, have showed signs for such a complicated magnetic phase diagram for these compounds [6,11–13]. Moreover, the complexity increases when a high magnetic field is applied. *i*-MAX samples with the RE elements Dy, Tb, and Ho were studied under high magnetic field by bulk magnetization, specific heat, x-ray absorption near edge structure, magnetic circular dichroism (for RE = Ho and Dy), and neutron diffraction [11,12]. The maximum applied magnetic field was in the range of 6–9 T. Both single crystal (RE = Ho and Dy [11]), and powder (Dy and Tb [12]) samples were studied. Magnetic-field and temperature phase diagrams were constructed for *i*-MAX compounds with RE = Dy and Ho, presenting new high-field magnetic phases in both cases. However, due to poor statistics (claimed by the authors) the exact nature of the high-field magnetic phase is inconclusive. In addition, the high-field magnetic structure was only studied at the lowest temperature (2 K) and not its temperature dependence.

NMR and frequency-dependent AC susceptibility are especially useful for determining the dynamics and magnetic phase diagram of magnetic materials at high magnetic fields. These methods have yet to be used in the study of *i*-MAX compounds. High-magnetic-field measurements enable better understanding of magnetic materials, especially those with complex magnetic behavior such as *i*-MAX compounds, as the field can serve as a tool for disentangling degenerated electronic states. In addition, as a local probe measurement, NMR measures the local field distribution inside the sample, via the hyperfine interaction, hence allowing to gain a better understanding of the nature of magnetism of *i*-MAX samples, especially at high magnetic fields. Furthermore, this method can distinguish between the contributions of the main phase, and those of any magnetic impurities to the magnetic signal.

In the following, we show AC susceptibility and NMR measurements of *i*-MAX compounds of the form $(Mo_{2/3}RE_{1/3})_2AlC$, where RE = Gd, Dy, Ho, and Er. Note that for clarity, in the following, we use the term "RE-*i*" instead of the exact chemical formula. Our measurements agree with the existence of high-field magnetic phase for Dy-*i* and Ho-*i* but clearly show significant extension to high temperatures (up to 50 K in Ho-*i*). Moreover, this phase grows

in the temperature-field phase space as the RE atomic number increases until it dominates in Er-*i*. The high-field magnetic phase shows intriguing properties such as a magnetic phase transition which becomes more smeared and has an increasing transition temperature with an increasing magnetic field.

II. METHODS

A. Sample characterization

All samples used in this work are powder samples taken from batches that were prepared and characterized in a previous study [13]. Unfortunately, impurities exist in all RE-*i* samples reported to date by all research groups that studied powder samples. Since these impurities could contain RE and/or transition-metal elements, they might be magnetic, and therefore may influence the results. This issue was not addressed well enough in previous works and we find it vital to do so here. For that reason, a sample from each RE-*i* powder was remeasured by x-ray diffraction (XRD) and carefully reanalyzed for existence of impurities. The measurements were performed on a Bruker D2 diffractometer, at the Nuclear Research Centre, Negev, Israel, in the $2\theta = 7^\circ$–109° range with a step size of $\Delta 2\theta = 0.01^\circ$. Significant impurities are listed in Table S1 in the Supplemental Material [14] (for XRD data see Ref. [13]). Most of these impurities have a transition temperature below 10 K and are not expected to significantly affect the AC susceptibility and NMR measurements, since the transition temperatures of most RE-*i* compounds measured are higher than those of the impurities. Two exceptions should be noted: the ferromagnetic (FM) compound $GdAl_2$ ($T_c = 170$ K [15], ≈0.7 wt%) in the Gd-*i* sample, and the superconducting Mo_3Al_2C ($T_c = 9.2$ K [16]), which is found in Ho-*i* and Er-*i*.

B. Magnetic susceptibility and NMR measurements

To thoroughly characterize the high-field magnetic phase diagram of *i*-MAX samples, AC susceptibility and NMR measurements were performed. AC susceptibility was measured using the PPMS AC susceptibility option (Quantum Design) at the Physics Department of Ben-Gurion University, Israel. The measurements were made in the temperature range of $T = 3$–300 K and field range of $\mu_0 H = 0$–9 T. For the AC susceptibility measurements, three frequencies were used: 0.75, 3.5, and 10 kHz. Anomalies in the AC susceptibility curves appear at temperatures that were determined by the maximum of the real susceptibility $\chi'(T)$, while some data points were determined by fitting a double Gaussian to $\chi'(T)$ where the anomaly was broad. NMR measurements were made at the National High Magnetic Field Laboratory located at Tallahassee, FL. Field-swept Al-27 NMR spectra were obtained in the field range $H = 0$–17 T for temperatures between $T = 4$–150 K, in a variable temperature cryostat. The NMR spectra were obtained by summing the Fourier transforms of spin-echoes and plotted as a function of magnetic field.

III. RESULTS

A. AC susceptibility

AC susceptibility results of Gd-*i*, Dy-*i*, Ho-*i*, and Er-*i* samples are marked throughout the paper (excluding Fig. 1) by blue, green, orange and red colors, respectively. Typical temperature-dependent measurements are shown in Fig. 1 for several fields.

Upon cooling down, the AC susceptibilities in all samples monotonically increase in a Curie-Weiss-like behavior, followed by anomalies at lower temperatures, characterized by nonmonotonic behavior of $\chi'(T)$. These anomalies can be classified according to their width along the temperature axis. The sharp anomalies, which exist also at zero-field, generally refer to spontaneous magnetic ordering, or to field-induced magnetic transitions. The broad anomalies may be related to crystalline electric field (CEF) effects [11]. However, this explanation is highly unlikely for a number of reasons. First, the change in occupation of the CEF energy levels by the magnetic field is expected to produce a broad maximum in $\chi'(T)$, which appears at lower temperatures with increased field [17], contrary to what is observed. Second, it contradicts NMR (see below) and Neutron scattering [11] measurements, which imply the existence of an ordered high-field magnetic phase. Third, an evolution of the magnetic-field–temperature phase diagram is observed as the RE atomic number increases (Fig. 1), which is described in the following. Gd-*i* starts from a single sharp transition (≈26 K at zero-field) [6], which shifts to lower temperatures with increased magnetic field until it disappears completely. Note that at zero-field there is another sharp drop in the AC susceptibility of Gd-*i* (Fig. S1 in the Supplemental Material [14]), and Dy-*i* (Fig. S2 in the Supplemental Material [14]) below $T \approx 10$ K. This drop resembles a superconducting transition, and most likely originates from the superconducting Mo_3Al_2C or Mo_2C impurities. For $\mu_0 H \geqslant 3$ T, another sharp magnetic transition is observed, with a critical temperature of ≈30 K, which does not change significantly with an applied field. A similar low-temperature sharp transition can be seen for Dy-*i*. Unlike Gd-*i*, which shows a continuous decrease in the transition temperature, the temperature of this transition decreases for an applied field of $\mu_0 H < 1$ T, increases for $1 < \mu_0 H < 2$ T and finally decreases again for $\mu_0 H > 2$ T, with a slight increase observed again for $5 < \mu_0 H < 6.5$ T.

Next, a broad high-field anomaly appears for Dy-*i* for $\mu_0 H > 6$ T. Surprisingly, increasing the field results in an increase in the transition temperature, where $\chi'(T)$ gains a maximum. Similar behavior of $\chi'(T)$ is also observed in Ho-*i*, appearing for $\mu_0 H > 4$ T, while the low-temperature magnetic transition is truncated above this field.

Finally, Er-*i* shows a single broad magnetic anomaly. Surprisingly, the known low-temperature and low-field transition (≈5 K at zero-field, reported as 3.6 K in Ref. [6]) is suppressed with fields as small as 0.1 T (Fig. S4 in the Supplemental Material [14]). For $\mu_0 H \geqslant 2$ T a broad maximum appears in $\chi'(T)$ whose peak temperature increases while increasing the field similarly to Dy-*i* and Ho-*i*.

B. NMR

Figure 2 shows various NMR measurements made on Gd-*i*, Dy-*i*, and Ho-*i* samples. The spectra are plotted as a function of the rescaled field:

$$H_N = (\omega_0/\gamma \times H) - 1, \tag{1}$$

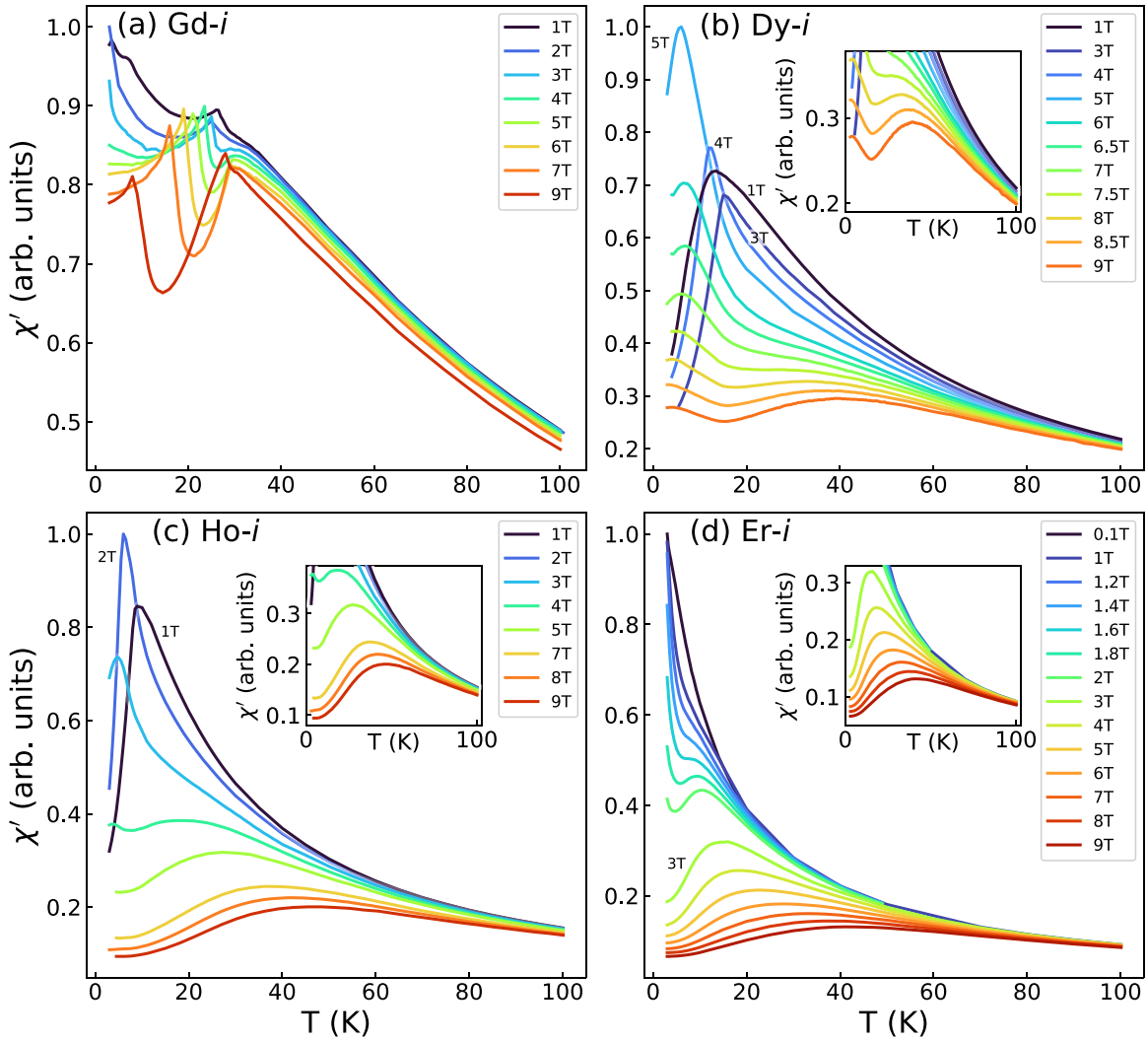

FIG. 1. AC susceptibility temperature scans. AC susceptibility measurements (χ') as a function of temperature (normalized with respect to the highest measured value). Upon cooling, a Curie-Weiss-like behavior is observed followed by anomalies at lower temperatures. (a) Gd-i = $(Mo_{2/3}Gd_{1/3})_2AlC$ with two anomalies that persist up to $\mu_0 H = 9\,T$. (b) Dy-i = $(Mo_{2/3}Dy_{1/3})_2AlC$ with a single anomaly below $\mu_0 H = 5\,T$ that is stable up to $\mu_0 H = 9\,T$. Around $\mu_0 H = 6\,T$ a second anomaly emerges that shows an increasing T_c and broadens with the field. (c) Ho-i = $(Mo_{2/3}Ho_{1/3})_2AlC$ with a single anomaly below $\mu_0 H = 3\,T$, stable up to $\mu_0 H = 4\,T$, where a second anomaly emerges and shows similar H-dependent behavior as in Dy-i. (d) Er-i = $(Mo_{2/3}Er_{1/3})_2AlC$ with a single anomaly that also shows similar H-dependent behavior as Dy-i and Ho-i. Insets are zoom-in on the "high-field anomalies" in Dy-i (b), Ho-i (c), and Er-i (d). All show a similar behavior with a new anomaly entering that increases with the field and becomes broader while decreasing the signal (χ'). All measurements were made using a frequency of $F = 10\,kHz$ for $0.1\,T \leqslant \mu_0 H \leqslant 9\,T$. Most measurements were performed in the temperature range of $T = 3$–$100\,K$. Additional measurements were also performed at a frequency of $F = 0.75\,kHz$ (not shown) with similar results.

where ω_0 is the spectrometer frequency and γ is the gyromagnetic ratio of the Al-27 nucleus ($\gamma = 11.094\,MHz/T$). Note that this plot automatically captures the value of the effective Knight shift relative to a bare nucleus. All measurements shown in Fig. 2(d) were made at $T = 4.2\,K$, while sweeping the field in the range $\mu_0 H = 7$–$10\,T$.

A clear double-peak line-shape can be recognized from Fig. 2 only for several measurements of Dy-i and for all measurements of Ho-i. In contrast, Gd-i [Fig. 2(d)] shows a broad line-shape which most likely originates from the overlap of two peaks. Note also that the double-peak structures observed are negatively shifted. In addition, for Dy-i, a triple peak can be seen for the lower field measurements [Fig. 2(b)], as evidenced by the low field (near $H_N = 0.2$, $H = 3$–$6\,T$) shoulder of the central peak. This triple peak, approximately symmetric line-shape, turns into an asymmetric double peak structure while increasing the field. Finally, Ho-i exhibits a clear double-peak structure, which is shifted to negative fields, at high external fields (13–15 T), up to a temperature of $T = 30\,K$ [Fig. 2(c)]. The meaning of these NMR line-shapes is explained below in the discussion section.

IV. DISCUSSION

The field-temperature magnetic phase diagram of the RE-i compounds can be constructed from the AC susceptibility measurements by finding the maximum points of each measurement (Fig. 3). Here we assume that all anomalies

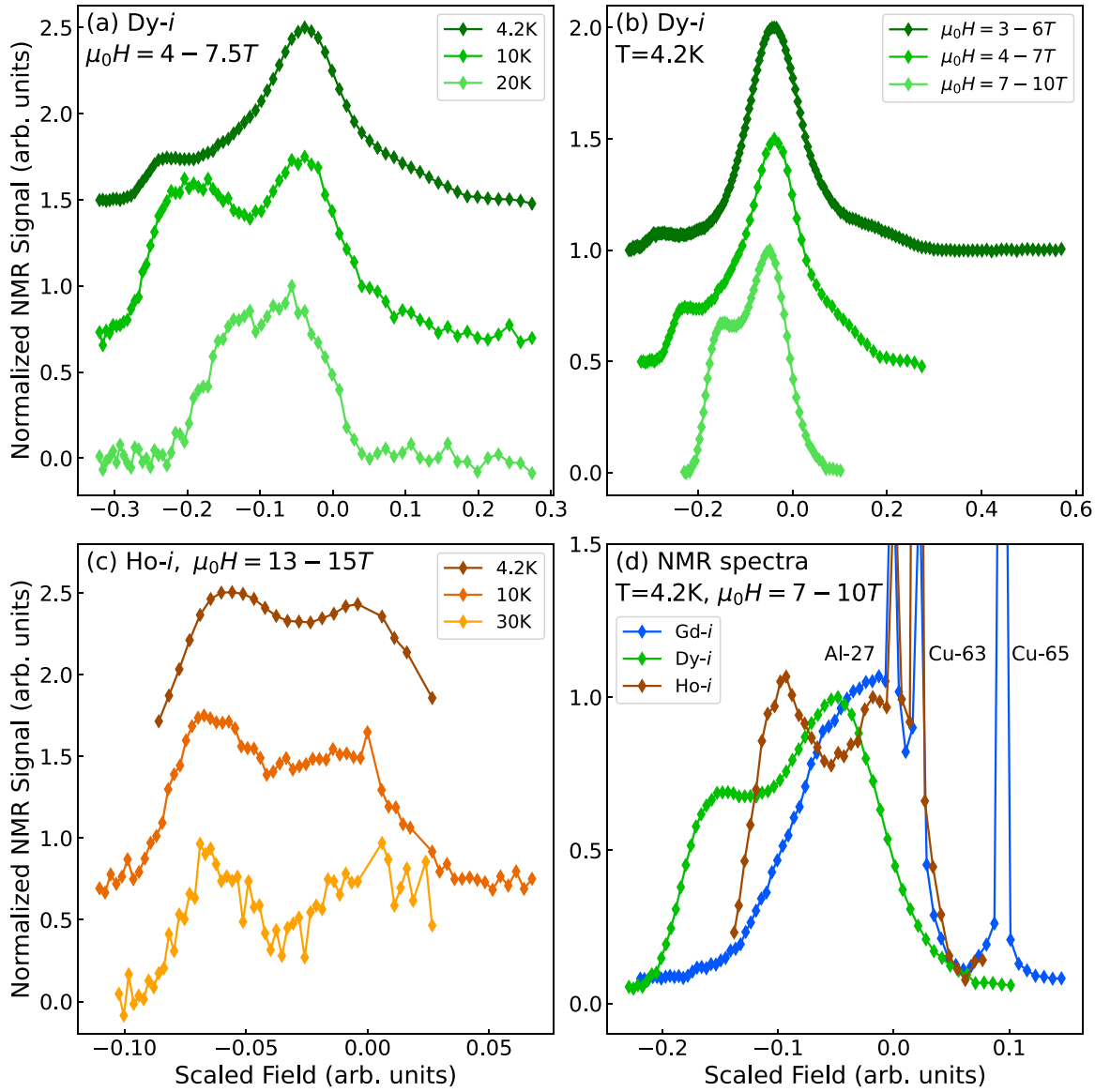

FIG. 2. NMR magnetic-field scans. (a) NMR Field sweep Dy-*i* measurements. Various Dy-*i* field sweep measurements, taken at different temperatures. All measurements were obtained at a frequency of 56.5 MHz and in the field range $\mu_0 H = 4$–7.5 T. (b) NMR field sweep measurements of Dy-*i*. All measurements were done at a temperature of $T = 4.2$ K. (c) NMR temperature dependence Ho-*i* measurements. All measurements were performed at a frequency of $F = 148$ MHz, corresponding to a field range between $\mu_0 H = 13$–15 T. Data presented in panels (a)–(c) is offset along the y axis for clarity. (d) Normalized Al-27 NMR spectra in Gd-*i*, Dy-*i*, and Ho-*i*. All measurements were performed at $T = 4.2$ K for a field span between 7–10 T. The sharp peaks seen in the spectra are attributed to either Copper (coming from the NMR coil) or residual Aluminum in the samples. All the spectra presented in (a)–(d) are plotted as a function of the re-scaled field: $H_N = (\omega_0/\gamma \times H) - 1$, see Eq. (1) in the text.

measured by AC susceptibility are due to magnetic phase transitions. In Fig. 3 the open data points were taken by the AC susceptibility's maximum, and the closed (transparent) data points were taken from fitting a double-Gaussian to the broad peak data. The difference between the phase diagrams of the different compounds measured is striking. Especially, the effects of an applied magnetic field on the critical temperatures of the magnetic phases.

Gd-*i* has the lightest RE element measured in this work. Therefore, it is logical to start the discussion with it, and search for evolution in the magnetic properties as we proceed to heavier REs. The zero-field magnetic properties of Gd-*i* were determined in previous studies [6,13]. It orders magnetically in zero magnetic field below $T = 26$ K [6]. This magnetic state was shown to be a commensurate antiferromagnet (AFM) [13]. The transition temperature of this magnetic state is suppressed by increasing the magnetic field. At $\mu_0 H = 3$ T another magnetic transition appears near $T = 30$ K. This transition is stable at least up to a field of $\mu_0 H = 10$ T, as measured by AC susceptibility [up to 9 T, Fig. 1(a)], and NMR [Fig. 2(d)]. Note that for an AFM structure, we expect to measure a NMR double-peak structure. However, the broad nonsymmetric NMR line-shape measured is probably the combination of two broad peaks together with a

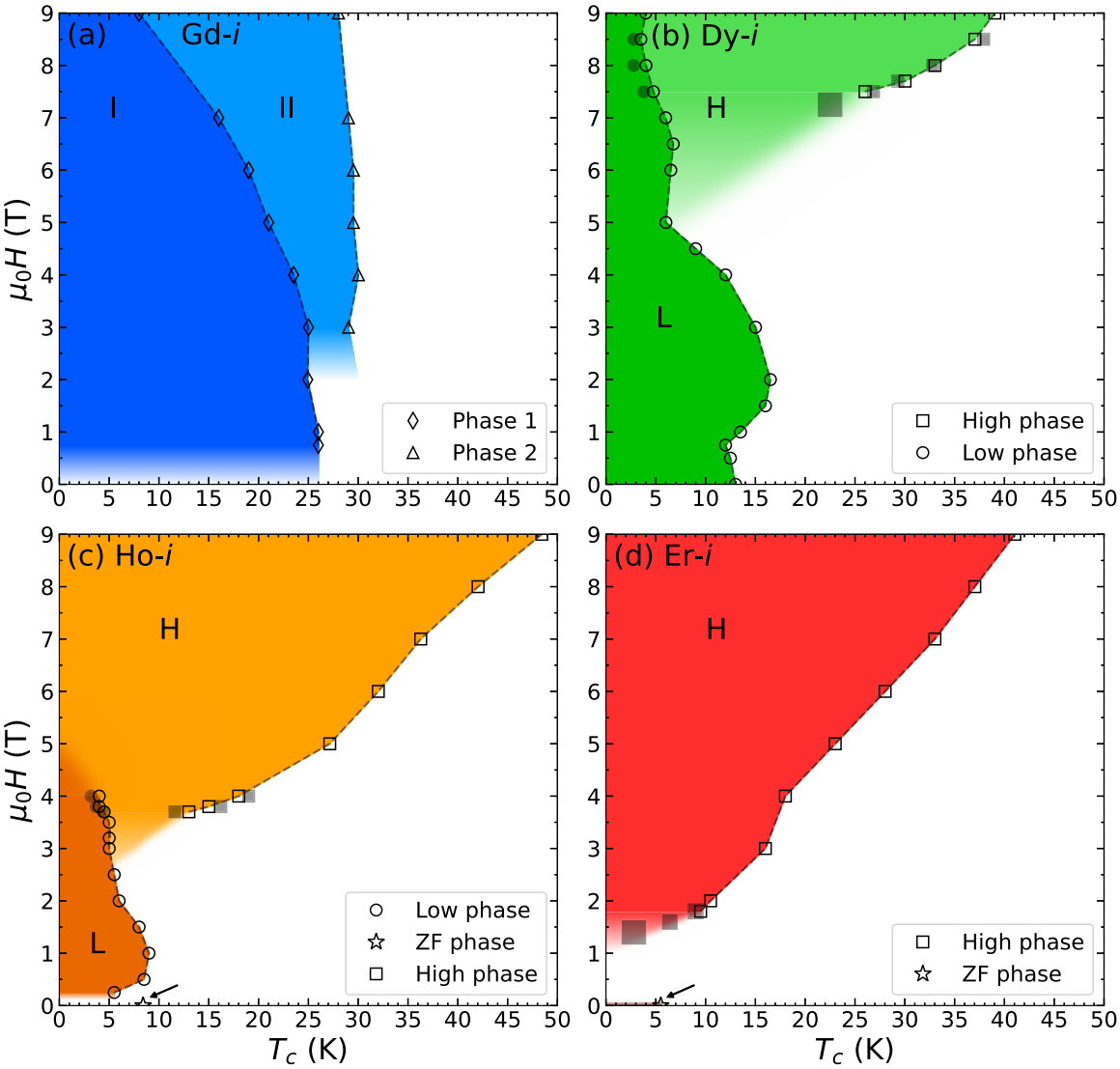

FIG. 3. Phase diagram. Phase diagram for each of the RE-*i* samples with RE = (a) Gd, (b) Dy, (c) Ho, and (d) Er marked by blue, green, orange, and red colors, respectively. A clear evolution of the magnetic structure of matter while increasing RE is evidenced. Specifically, from two competing magnetic phases (Gd-*i*, phases 1 and 2) existing for a large portion of the H–T phase, into a formation of a new high-field–high-temperature (high BT, marked as H) phase is shown (Dy-*i*/Ho-*i*/Er-*i*), where the high-field phase seems to come at the expense of the lower one (marked as L), until for Er-*i* the low phase totally disappears. The arrow in panels (c) and (d) refers to the ZF phase seen in Figs. S3 and S4 (Supplemental Material [14]). All diagrams were plotted for a frequency of $F = 10$ kHz. The gradient of the colors and the blur are a guide to the eye showing where the phase transition is still growing and there is a large uncertainty about the location of the phase transition. The size of the markers is larger or equal to the error-bars for simplicity.

significant FM component emerging either from a $GdAl_2$ magnetic impurity or from a canted AFM state in Gd-*i*.

Interestingly, while examining the higher RE elements starting with Dy-*i*, we reveal a very different picture than what is observed for Gd-*i*. Initially, at low fields, the Dy-*i* shows a dual transition at $T = 9$ and 13 K at zero magnetic field seen in Fig. S2 (see Supplemental Material [14]). The $T = 13$ K transition matches the transition reported in the literature [6,11]; however, the $T = 9$ K transition might be due to the Mo_3Al_2C impurity, which becomes superconducting at $T = 9.2$ K. Note also that no match for the transition at $T = 16$ K, mentioned in the literature [6], was found in the current AC susceptibility measurements. This may be due to smearing of the transition, by orientational averaging in powder samples. In addition, the transitions mentioned in the literature show slim changes in the signal of the magnetization [6,11]. The lower transition is observed only up to a field of $\mu_0 H = 0.5$ T. The higher-field anomaly stretches at least up to $\mu_0 H = 9$ T. Note that at a field of $\mu_0 H = 5$, T a significant drop in transition temperature has been observed for the low-field transition, probably due to the magnetic moment saturation reported in Ref. [11]. We claim that this presumable moment saturation is actually a transition to another magnetic state, as will be explained below. Specifically and surprisingly, at the same point (near $H = 5$ T) another high-field magnetic anomaly emerges. The transition temperature of this purported new magnetic state is enhanced at higher fields. This behavior is opposite to both Gd-*i* and Tb-*i* (see Ref. [18],

results not shown in this manuscript), which show a decrease in the anomaly temperature at high fields. In addition, NMR measurements [Fig. 2(b)] show a change in the of line-shape between the two phases, from a nearly symmetric triple-peak line-shape for low fields (low transition temperature phase), to a negatively shifted re-scaled field, double peak structure for the high-field phase, implying a canted nonsymmetric AFM. As seen in Fig. 2(b), the large peak near the resonance field for $\mu_0 H = 3$–$6\,\mathrm{T}$ field sweep measurements is probably due to the spin portion of the lattice, which is already aligned in the external field direction (canting AFM), while the two side peaks originate from the AFM state. While increasing the field, a double-peak emerges, indicating a reduced AFM hyperfine component [Fig. 2(b)]. This is accompanied by a slight increase in the FM (more negative shift) component which suggests further canting of the spins as the temperature is increased, and the sample shifts from the lower magnetic phase to the high-field phase. A similar change from low phase (AFM, $T = 4.2\,\mathrm{K}$) to high phase (canted AFM, $T = 10\,\mathrm{K}$) can also be recognized in Fig. 2(a), where increasing the temperature changes the Dy-*i* magnetic phase [see also Fig. 3(b)].

The Ho-*i* data shows a transition temperature of $T = 8.5\,\mathrm{K}$ at zero-field, identical to the transition temperature reported in Ref. [7], and close to that reported in Refs. [6,11]. This transition terminates at $\mu_0 H = 0.01\,\mathrm{T}$ and then reenters at $\mu_0 H = 0.3\,\mathrm{T}$, existing up to a field of $\mu_0 H \approx 4\,\mathrm{T}$, close to which a high-field magnetic transition emerges at $T = 13\,\mathrm{K}$. The transition temperature of this magnetic phase then increases with field, similar to the Dy-*i* high-field magnetic transition. Note that NMR measurements show the existence of this magnetic state at least up to a field of $\mu_0 H = 15\,\mathrm{T}$ at $T = 4.2\,\mathrm{K}$ [see Fig. 2(c)].

Finally, Er-*i* exhibits a low temperature transition ($T = 5.5\,\mathrm{K}$) at zero-field, similar to the $T = 3.6\,\mathrm{K}$ transition noted in the literature [6]. However, this transition disappears when the external field is increased to $\mu_0 H = 0.04\,\mathrm{T}$. At a field of $\mu_0 H = 2\,\mathrm{T}$ the high-field phase emerges, where increasing the field up to (at-least) $H = 9\,\mathrm{T}$ implies an increase in the transition temperature, similar to Dy-*i* and Ho-*i*.

All the above findings can be summarized in the high-field phase diagrams of Dy-*i* and Ho-*i* (Fig. 4). A comparison with previous literature results, taken using single crystals, is also presented, showing, in general, good agreement for the low-field phase [11]. Deviation from the literature [11] is observed mainly for the case where previous measurements were done with magnetic field aligned along the *a* axis, which serves as the easy axis in these compounds. This transition is probably smeared out when powder samples are measured, as is the case in this work.

The high-field–high-temperature phase is observed here for the first time for the RE-*i*-MAX phases. It is important to note that previous work did not study the magnetic field and temperature regions of our newly found high-field magnetic phase. Specifically, previous neutron diffraction studies, that were conducted on single crystals [11], focused on the limited q space region of the (0,q,0) reflections. Moreover, they were conducted in a relatively small section of the H-T magnetic phase diagram, not reaching the entire phase space we report here.

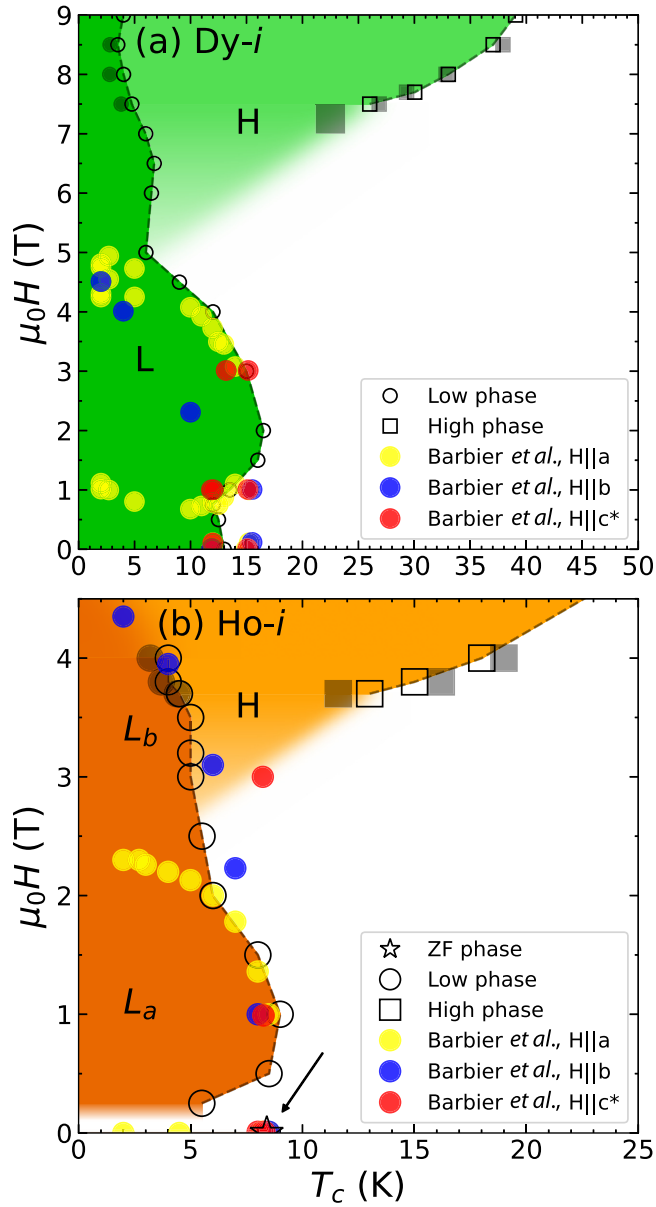

FIG. 4. Dy-*i* and Ho-*i* phase diagram comparison. AC susceptibility data measured for powder (a) Dy-*i* and (b) Ho-*i* samples showing the zero magnetic field (ZF), low- and high-temperature and magnetic-field phases (open star, circles, and squares, respectively). Thermodynamic and diffraction data measured for single crystal Ho-*i* samples in *a*, *b*, and *c* axes (yellow, blue, and red circles, respectively), taken from Barbier *et al.* [11]. Comparison of the present results to the previously published data [11] shows good agreement with the addition of the high-temperature and magnetic-field phases. Ho-*i* shows a clear distinction between the low phase in *a* or *b* directions, hence L_a and L_b referring to different contributes from *a*, *b* axes to the powder diagram. The Dy-*i* is more complicated hence was left with a single "L" marker.

These findings point to the emergence of a novel high-field magnetic phase. The universality of this phase for various *i*-MAX compounds is clear. This new magnetic phase has peculiar features, very different from the low magnetic phases already noted in previous studies [6,11]. Specifically, the

high-field phase, which has a significant FM component (i.e., a canted AFM) is different from the low-field magnetic phases. While the low-field magnetic phases show a typical behavior, in which the transition temperature drops with increasing magnetic field, the high-field phase shows the opposite.

In addition, the high-field phase transition becomes more smeared with increasing magnetic field. Note that the emergence of this high-field phase might be due to a competition between different magnetic phases, similar to the ones shown in Ref. [19]. There, while increasing the field, one magnetic order changes to another, more energetically favorable. Another hint on the nature of this high-field phase can be found in the evolution of the Ho-*i* phase diagram as a function of field measured by neutron diffraction [11]. Starting with an AFM structure, a FM component (i.e., a canted AFM) emerges for $\mu_0 H > 1\,\mathrm{T}$. This behavior develops with increased field along the *a* axis forming a canted AFM with a significant FM component for $\mu_0 H > 2\,\mathrm{T}$. Therefore, we hypothesize that the high-field phase found here has a large FM canting component, that becomes more prominent as the field increases. This magnetic transition appears at higher temperatures as the strength of the applied field increases probably due to stabilization effect of the FM component by field application. The NMR measurements support the above findings, as a significant double-peak structure, attributed to magnetically ordered canted AFM state (see also Ref. [20]), has been shown up to a field of $\mu_0 H = 10\,\mathrm{T}$ for Dy-*i* and $\mu_0 H = 15\,\mathrm{T}$ for Ho-*i*.

V. CONCLUSIONS

Our investigation of several *i*-MAX compounds using a variety of experimental techniques has revealed intriguing insights into their magnetic behavior. We uncovered a complex magnetic phase diagram featuring the reentrance of magnetic phases and the existence of a high-field phase. Notably, we observed contrasting behavior between Gd-*i* and Tb-*i* [18] compounds, where the ordered magnetic state weakens with increasing field, compared to Dy-*i*, Ho-*i*, and Er-*i*, where the transition temperature increases at least up to fields of 9 T. This increase is likely linked to the contraction of the unit cell, which suppresses the low-field phase and enhances the high-field phase. It is followed by the introduction of canted AFM order, with probable increase in the FM component significance, which survives even at fields as high as 17 T [for Ho-*i*, see Fig 2(c)]. This points to the uniqueness of the high-field phase in these materials. Our results indicate that a competition exists between different magnetic phases, with one phase becoming energetically more favorable as the external field increases, similar to the one shown in Ref. [19]. This behavior may explain the observed disappearance and subsequent reemergence of magnetic phases with increasing field.

Based on our findings and earlier studies [6,11,12], we propose the following picture of the magnetic state in $(Mo_{2/3}RE_{1/3})_2AlC$ compounds. In the ground state, the magnetic configuration is complex due to the geometrical frustration of RE atoms, leading to an antiferromagnetic spin density wave (AFM SDW) for most compounds at zero field [13]. As the field increases, a canted AFM lattice emerges, with a stabilized FM component that aligns along the easy *a* axis and persists even at high fields, up to 17 T as evident in Ho-*i*. Furthermore, increasing the atomic number of the RE elements leads to a decrease in inter-atomic distance [6]. From the results presented here, as well as from the zero-field transition temperatures presented elsewhere [6,13], it is clear that the interaction strength of the low-field phase diminishes as well, starting from Dy-*i*. These findings need to be further explored, theoretically as well as experimentally, since no direct exchange mechanism is expected. This means that the strength of the magnetic interaction does not have to decrease with decreasing lattice dimensions, and a more complicated correlation is expected. The application of an increasing magnetic field also leads to a reduction in the strength of the low-field phases, which eventually vanish for Er-*i*, while the high-field phase becomes increasingly stabilized (for Dy-*i* and above). This behavior likely stems from the stabilization of the FM component along the easy *a* axis under high magnetic fields. Additional measurements, particularly high-field neutron diffraction, are needed to precisely characterize the high-field behavior of *i*-MAX compounds and to further clarify the nature of these intriguing magnetic phases.

ACKNOWLEDGMENTS

Work by D.Y. and E.M. was performed with support from the European Research Council Grant No. ERC-101117478, the Israeli Science Foundation Grant No. ISF-885/23 and the PAZY foundation Grant No. 412/23. J.R. acknowledges funding from the Knut and Alice Wallenberg (KAW) Foundation for a Scholar Grant (No. 2019.0433). A portion of this work was performed at the National High Magnetic Field Laboratory, which is supported by National Science Foundation Cooperative Agreement No. DMR-2128556* and the State of Florida.

[1] M. W. Barsoum, The $M_{N+1}AX_N$ phases: A new class of solids, Prog. Solid State Chem. **28**, 201 (2000).

[2] M. Dahlqvist, M. W. Barsoum, and J. Rosen, MAX phases–Past, present, and future, Mater. Today **72**, 1 (2024).

[3] M. Naguib, M. W. Barsoum, and Y. Gogotsi, Ten years of progress in the synthesis and development of MXenes, Adv. Mater. **33**, 2103393 (2021).

[4] M. Dahlqvist, J. Lu, R. Meshkian, Q. Tao, L. Hultman, and J. Rosén, Prediction and synthesis of a family of atomic laminate phases with Kagomé-like and in-plane chemical ordering, Sci. Adv. **3**, e1700642 (2017).

[5] Q. Tao, M. Dahlqvist, J. Lu, S. Kota, R. Meshkian, J. Halim, J. Palisaitis, L. Hultman, M. W. Barsoum, P. O. Persson *et al.*, Two-dimensional $Mo_{1.33}C$ MXene with divacancy ordering prepared from parent 3D laminate with in-plane chemical ordering, Nat. Commun. **8**, 14949 (2017).

[6] Q. Tao, J. Lu, M. Dahlqvist, A. Mockute, S. Calder, A. Petruhins, R. Meshkian, O. Rivin, D. Potashnikov, E. N. Caspi

et al., Atomically layered and ordered rare-earth *i*-MAX phases: A new class of magnetic quaternary compounds, Chem. Mater. **31**, 2476 (2019).

[7] J. Yang, G. Yao, S. Sun, Z. Chen, S. Yuan, K. Wu, X. Fu, Q. Wang, and W. Cui, Structural, magnetic properties of in-plane chemically ordered $(Mo_{2/3}R_{1/3})_2AlC$ (R = Gd, Tb, Dy, Ho, Er, and Y) MAX phase and enhanced capacitance of $Mo_{1.33}C$ MXene derivatives, Carbon **179**, 104 (2021).

[8] J. Yang, R. Liu, N. Jia, K. Wu, X. Fu, Q. Wang, and W. Cui, Novel W-based in-plane chemically ordered $(W_{2/3}R_{1/3})_2AlC$ (R = Gd, Tb, Dy, Ho, Er, Tm and Lu) MAX phases and their 2D $W_{1.33}C$ MXene derivatives, Carbon **183**, 76 (2021).

[9] S. Sun, Z. Ma, Z. Chen, P. Liu, Y. Song, Q. Lu, X. Fu, Q. Wang, and W. Cui, The crystallographic structure and properties of novel quaternary nanolaminated rare-earth-Cr-based *i*-MAX phases, Acta Mater. **242**, 118479 (2023).

[10] Z. Chen, H. Chong, S. Sun, J. Yang, G. Yao, Q. Wang, J. Zhu, S. Yang, and W. Cui, Synthesis and characterizations of solid-solution *i*-MAX phase $(W_{1/3}Mo_{1/3}R_{1/3})_2AlC$ (R = Gd, Tb, Dy, Ho, Er and Y) and derivated i-MXene with improved electrochemical properties, Scr. Mater. **213**, 114596 (2022).

[11] M. Barbier, F. Wilhelm, C. V. Colin, C. Opagiste, E. Lhotel, D. Pinek, Y. Kim, D. Braithwaite, E. Ressouche, P. Ohresser *et al.*, Magnetic properties of the $(Mo_{2/3}R_{1/3})_2AlC$ (R = Ho, Dy) *i*-MAX phases studied by x-ray magnetic circular dichroism and neutron diffraction, Phys. Rev. B **105**, 174421 (2022).

[12] Q. Tao, M. Barbier, A. Mockute, C. Ritter, R. Salikhov, U. Wiedwald, S. Calder, C. Opagiste, R.-M. Galera, M. Farle *et al.*, Magnetic phase diagram of $(Mo_{2/3}RE_{1/3})_2$ AlC, RE = Tb and Dy, studied by magnetization, specific heat, and neutron diffraction analysis, J. Phys.: Condens. Matter **34**, 215801 (2022).

[13] D. Potashnikov, E. Caspi, A. Pesach, Q. Tao, J. Rosén, D. Sheptyakov, H. Evans, C. Ritter, Z. Salman, P. Bonfa *et al.*, Magnetic structure determination of high-moment rare-earth-based laminates, Phys. Rev. B **104**, 174440 (2021).

[14] See Supplemental Material at http://link.aps.org/supplemental/10.1103/PhysRevB.111.094427 for summary of impurity analysis; and additional ac susceptibility low-magnetic-field temperature scans, which also contains Refs. [21–23].

[15] D. S. Williams, P. M. Shand, T. M. Pekarek, R. Skomski, V. Petkov, and D. L. Leslie-Pelecky, Magnetic transitions in disordered $GdAl_2$, Phys. Rev. B **68**, 214404 (2003).

[16] A. B. Karki, Y. M. Xiong, I. Vekhter, D. Browne, P. W. Adams, D. P. Young, K. R. Thomas, J. Y. Chan, H. Kim, and R. Prozorov, Structure and physical properties of the noncentrosymmetric superconductor Mo_3Al_2C, Phys. Rev. B **82**, 064512 (2010).

[17] H. S. Lee, H. B. Kim, R. E. Kim, W. C. Ri, B. K. Cho, and J. J. Oh, Crystalline electric field effects and magnetic properties of $Ho_{1-x}Dy_xNi_2B_2C$ single crystals, J. Korean Phys. Soc. **34**, 88 (1999).

[18] D. Yahav, D. Potashnikov, A. Pesach, O. Rivin, E. N. Caspi, J. Rosen, M. Schechter, A. Maniv, and E. Maniv, Field-induced spin dynamics in *i*-MAX Tb compound, arXiv:2501.01520.

[19] S. C. Haley, S. F. Weber, T. Cookmeyer, D. E. Parker, E. Maniv, N. Maksimovic, C. John, S. Doyle, A. Maniv, S. K. Ramakrishna *et al.*, Half-magnetization plateau and the origin of threefold symmetry breaking in an electrically switchable triangular antiferromagnet, Phys. Rev. Res. **2**, 043020 (2020).

[20] E. Maniv, R. A. Murphy, S. C. Haley, S. Doyle, C. John, A. Maniv, S. K. Ramakrishna, Y.-L. Tang, P. Ercius, R. Ramesh *et al.*, Exchange bias due to coupling between coexisting antiferromagnetic and spin-glass orders, Nat. Phys. **17**, 525 (2021).

[21] N. Morton, B. James, G. Wostenholm, D. Pomfret, M. Davies, and J. Dykins, Superconductivity of molybdenum and tungsten carbides, J. Less-Common Met. **25**, 97 (1971).

[22] A. Boutahar, R. Moubah, E. Hlil, H. Lassri, and E. Lorenzo, Large reversible magnetocaloric effect in antiferromagnetic Ho_2O_3 powders, Sci. Rep. **7**, 13904 (2017).

[23] V. Narang, D. Korakakis, and M. Seehra, Nature of magnetism and magnetic-field-induced transitions in non-collinear antiferromagnet Er_2O_3, J. Magn. Magn. Mater. **368**, 353 (2014).